RSC Advances

PAPER

View Article Online
View Journal | View Issue

Cite this: *RSC Adv.*, 2025, **15**, 15190

A fluorescent probe based on a luminescent metal–organic framework for the sensitive detection of histamine in aquatic products†

Mei Zhou,[a] Simiao Zhang,[b] Shihuang Wang,[b] Yutong Huang,[a] Xiaokang Xu,[a] Weiqing Sun,[a] Qiaozhen Liu[a] and Jing Ma *[a]

An effective way to prevent histamine poisoning is to assess the safety of aquatic products, and hence, developing a new method for detecting histamine is particularly important. In this study, a fluorescence probe (AgNPs@PCN-224) was constructed for the sensitive detection of histamine by utilizing the mesoporous structure of a zirconium porphyrin metal–organic framework (PCN-224) loaded with silver nanoparticles (AgNPs). Because PCN-224 and AgNPs were close to each other, there was a fluorescence resonance energy transfer between the two substances, resulting in fluorescence quenching. At this point, under the action of diamine oxidase, the decomposition product of histamine (hydrogen peroxide) etched the silver nanoparticles onto the surface of PCN-224, and the fluorescence of PCN-224 was recovered. Under optimal conditions, it was confirmed that the fluorescence intensity of the probe was positively correlated with the histamine concentration in the range of 10–100 μM, with a correlation coefficient of 0.9527, and the detection limit was calculated to be 0.033 nM. The detection performance for hydrogen peroxide was also investigated, and the results demonstrated that the probe was suitable for dual-substance detection of both histamine and hydrogen peroxide. Finally, when used for the detection of grass carp samples, it was found that the recovery rate ranged from 98% to 110%, with a relative standard deviation below 8%. The findings confirmed the reliability of the AgNPs@PCN-224 fluorescent probe established in this study for the detection of histamine in aquatic samples.

Received 12th February 2025
Accepted 13th April 2025

DOI: 10.1039/d5ra01025j

rsc.li/rsc-advances

Introduction

Biogenic amines (BAs) are biologically active natural alkaline nitrogen compounds that are catalyzed by microbial histidine decarboxylase in a variety of foods.[1,2] Among them, histamine (His) is one of the most representative biological amines, which is commonly found in aquatic and fish foods and is produced by bacteria through the catalytic action of histidine decarboxylase.[3] Normally, it acts as a "regulator" of immune responses, neurotransmitters and physiological functions.[4] However, its excess consumption can lead to allergic food poisoning (histamine poisoning), triggering a series of diseases, such as headaches, diarrhea, hypotension, and respiratory disturbances.[5–7] As the primary amine in fish, its content has been recognized as an indicator for assessing fish spoilage, with a prescribed limit of 50 mg kg^{-1}.[8–10] It is present in a wide range of food sources, and traditional processing methods are unable to disrupt its structure.[11,12] Therefore, timely and accurate monitoring of histamine is the key to preventing histamine poisoning. Given the complexity and trace nature of many food components, the development of rapid and sensitive histamine detection techniques is a challenge.

At present, the detection of His relies on traditional chromatography techniques, such as high-performance liquid chromatography (HPLC) and thin-layer chromatography (TLC), and these techniques require highly sophisticated instruments, skilled personnel and dedicated operation sites, making it impossible to achieve rapid and on-site detection.[13–17] In contrast, optical sensing technology offers a faster and simpler detection method.[18,19] With the emergence of superior nanoparticles, such as metal nanoclusters, up-conversion nanoparticles and metal–organic frameworks, optical sensing technology has made significant impacts in many fields, especially in food safety, ecology and environment, and biomedicine.[20,21] This has been accompanied by a boom in visual detection and real-time analysis technology. For example, Yao's group[22] established an optical sensor that combines colorimetric and fluorescence techniques for formaldehyde detection, which they propose as a candidate for formaldehyde pollutant detection. Also, Chen *et al.*[23] proposed a sensor based on colorimetric, fluorescence and photothermal triple-mode

[a]*College of Life Science, Yangtze University, Jingzhou, Hubei 434023, People's Republic of China. E-mail: majing@yangtzeu.edu.cn; Fax: +0716-8066182; Tel: +0716-8066182*
[b]*Jingzhou Institute for Food and Drug Control, Jingzhou, Hubei 434000, People's Republic of China*

† Electronic supplementary information (ESI) available. See DOI: https://doi.org/10.1039/d5ra01025j

detection to determine the content of rosmarinic acid (a food additive) in a variety of foods, with good results. Inspired by these previous works, we chose an MOF with excellent physical and fluorescent properties as the sensing platform, namely PCN-224.

The zirconium-based metal–organic framework PCN-224 belongs to a class of three-dimensional network compounds composed of zirconium ions interlinked with porphyrin ligands with a conjugated ring structure.[24,25] Thanks to the strong interactions between the carboxylate groups and zirconium as well as the large Stokes shifts induced by the porphyrins and their derivatives, PCN-224 exhibits strong physical and thermal stability as well as excellent optical properties.[26,27] In addition, based on its mesoporous structure with a large specific surface area and high porosity, the adsorption and recognition ability of PCN-224 is also noteworthy.[28–31] Currently, PCN-224 is popular among researchers as a potential platform for encapsulating biomolecules and nanoparticles.[32,33] Considering this, we chose PCN-224 for study and silver nanoparticles for its modification. Silver nanoparticles (AgNPs), as typical metal nanoparticles with localized surface plasmon resonance and high extinction coefficient properties, are often used as electron donors in fluorescence resonance energy transfer (FRET) approaches applied for the construction of sensing platforms.[34,35] In particular, FRET is the main signal transduction mechanism of fluorescent sensors. For example, Zhang's group[36] prepared a sensitive fluorescent nanomaterial, namely MSNs@R6G-MnO_2, based on FRET between MSNs and R6G. In previous studies, various harmful substances have been successfully applied for PCN-224 detection, including porcine epidemic diarrhea virus, antibiotics, metal ions and organophosphorus pesticides.[35,37–40] However, to the best of our knowledge, PCN-224 has not yet been utilized for the detection of aquatic histamine.

In this work, a simple and efficient fluorescence probe, namely AgNPs@PCN-224, was constructed for the specific detection of histamine. As shown in Fig. 1, Zr^{2+} metal ions and TCPP organic ligands were used as the precursors of PCN-224, which was prepared by a traditional hot solvent method, and acted as the carrier of AgNPs and generated the output signal of the system. A PCN-224 probe loaded with AgNPs, namely AgNPs@PCN-224, was then obtained by a one-pot thermal method using sodium borohydride to reduce silver nitrate *in situ*. This process triggered FRET between the two substances, resulting in the quenching of the fluorescence of PCN-224. Since diamine oxidase can specifically degrade diamine (histamine), when diamine oxidase was introduced into the detection system, the hydrogen peroxide product oxidized the silver nanoparticles to silver ions and stripped them from PCN-224, thereby blocking the FRET and restoring the fluorescence. Therefore, the histamine concentration could be quantified in a certain range according to the amount of fluorescence recovery. Furthermore, based on the sensing mechanism, we concluded and confirmed that the probe was also suitable for the detection of the product hydrogen peroxide. Finally, the application of the developed probe to analyze grass carp samples demonstrated that the AgNPs@PCN-224 probe could be used as a reliable and new strategy for histamine analysis in aquatic products.

Experimental section

Chemicals and materials

Meso-tetra(4-carboxyphenyl)porphin (TCPP) was purchased from Chemical Industry Development Co. (Shanghai). Diamine oxidase (DAO), histamine (His), putrescine dihydrochloride (Put) and cadaverine dihydrochloride (Cad) were provided by Sigma-Aldrich (Shanghai, China). Cysteine was obtained from Beijing Auboxin Biotechnology Co. The other reagents, such as $ZrOCl_2 \cdot 8H_2O$, $AgNO_3$, $NaBH_4$, benzoic acid and *N*,*N*-dimethylformamide (DMF), were purchased from Sinopharm Chemical Reagent Co., Ltd (Shanghai, China). The fresh grass

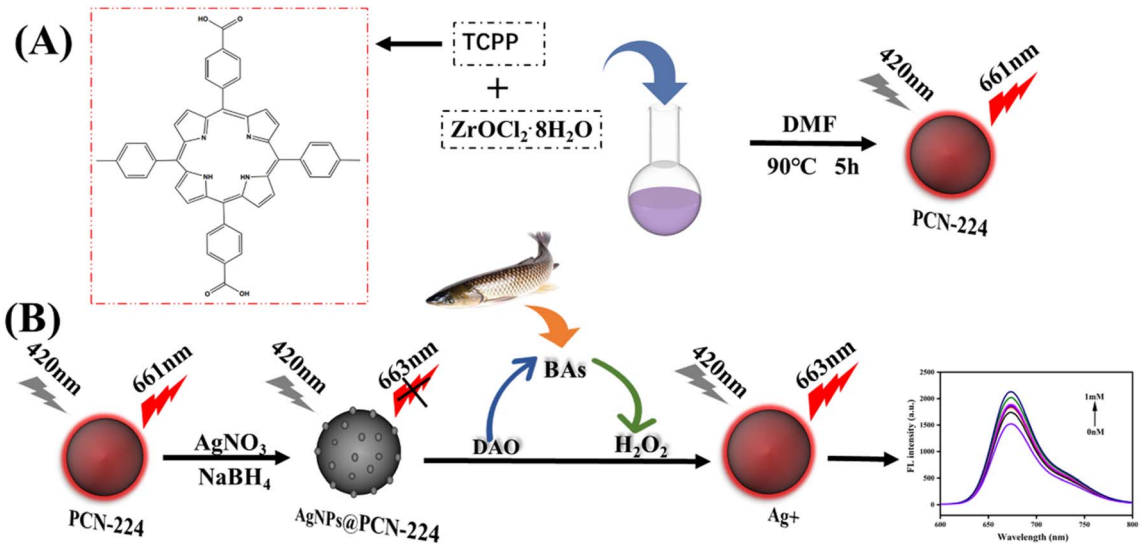

Fig. 1 (A) Preparation of PCN-224. (B) Schematic of AgNPs@PCN-224 for constructing a biosensor to detect histamine.

carp samples were purchased from a local supermarket for the subsequent tests for the detection of His in real samples. All the solvents were of analytical grade and used without further purification. Ultrapure water provided by a Millipore system (USA) was used throughout all the experiments.

Methods

Fluorescence, Fourier transform infrared (FT-IR) and UV-visible light absorption spectroscopies were performed using an F-7000 fluorescence spectrophotometer (Japan), IR-960 infrared spectrophotometer (China) and TU-1900 dual beam UV-visible spectrophotometer (China), respectively. TEM images were recorded using an HT-7800 TEM system (Japan). Fluorescence observations were obtained using a ZF-7 cassette Triple UV analyzer. Thermogravimetric (TG) analysis was conducted using a thermogravimetric analyzer (JY-TGA610). To confirm the crystal phases of the materials, X-ray diffraction patterns were recorded in the range of 5–50° using a Bruker D8 Advance XRD system. The Brunauer–Emmett–Teller adsorption isotherms and particle-size distribution measurements were recorded using a Micromeritics ASAP 2460 system. The fluorescence lifetimes of the fluorescent substances were measured using an Edinburgh Instruments FLS1000 system.

Synthesis of PCN-224

PCN-224 was synthesized using a traditional hot solvent method.[37] In the typical procedure, 10 mg TCPP, 30 mg $ZrOCl_2$ and 220 mg benzoic acid were homogeneously mixed and dissolved in DMF (10 mL) under ultrasonic conditions, and then transferred into a 50 mL round-bottomed flask, which was placed in a 90 °C oil bath and the mixture stirred for 5 h. At the end of the reaction, a dark purple-colored solution was obtained, which was allowed to cool naturally and was then fully washed with DMF three times to wash away any unreacted material. Finally, dark-purple-colored PCN-224 powder was obtained after drying overnight.

Synthesis of AgNPs@PCN-224

Under the optimal conditions, AgNPs@PCN-224 was prepared by a simple solvothermal method. Briefly, ready-made $AgNO_3$ (100 μL, 2.5 mM) was added to the as-synthesized PCN-224, and the solution was magnetically stirred at 25 °C for 1 h. Subsequently, $NaBH_4$ (25 μL, 0.1 M) was instantly added and allowed to react for 3 h. After that, silver-modified PCN-224 nanoparticles (AgNPs@PCN-224) were obtained after centrifugally washing the precipitate for 20 min at 14 000 rpm.

Detection of histamine

The enzyme-mediated reaction requires tightly controlled reaction conditions, which were thus explored for determining the optimum enzyme concentration, temperature, pH and time. A fixed concentration of DAO solution (20 mg mL^{-1}) was added to different a concentrations of histamine solution with a mixing volume ratio of 1 : 1 and incubated at 30 °C for 40 min. Then the above reaction solution was added to 1 mL of AgNPs@PCN-224 suspension followed by incubation at 35 °C for 30 min. The fluorescence spectrum was measured at an excitation wavelength of 420 nm, and the fluorescence intensity at 663 nm was recorded, utilizing a slit width of 5.0 nm and a photomultiplier voltage of 600 V.

Pre-treatment of the samples

To assess the potential practicability of the AgNPs@PCN-224 probe, local grass carp was selected as a real sample. The sample was first pretreated according to a procedure described in previous literature with minor modifications.[41] First, 20 g of ground fish meat was mixed with trichloroacetic acid (3%, 20.0 mL). Next, vortex extraction at high speed for 5 min and centrifugation at 10 000 rpm for 10 min were applied to stratify the components. Then, the supernatant was taken and *n*-hexane (20 mL) was added followed by further high-speed vortexing (5 min), and finally the fat was removed. The sample was then allowed to stand and the lower solution was finally collected. The pH of this solution was then adjusted to neutral with NaOH solution and then the solution was diluted to 10 mL with PBS. Next, fluorescence detection was performed by replacing the histamine solution with the sample solution according to the measurement method described above. Finally, the reliability of the method was further verified by adding a certain amount of histamine standard solution to the sample and performing spiked recovery experiments.

Results and discussion

Characterization of AgNPs@PCN-224

The AgNPs@PCN-224 probe was prepared with reference to previous studies and optimized.[42] Given that AgNPs act as electron donors in FRET, and their stability and optical properties are closely related to the sensitivity of the fluorescence probe, we optimized their synthesis conditions one by one, including time, temperature, pH, and the concentration of Ag^+, and the results are shown in the ESI Data (Fig. S1).† The PCN-224 and AgNPs@PCN-224 were confirmed by electron microscopy (Fig. 2). Fig. 2A shows that pure PCN-224 was elliptical in shape, and uniformly distributed in water without significant aggregation. On the contrary, due to the modification of PCN-224 by AgNPs, the surface of AgNPs@PCN-224 became rough and the loading phenomenon of AgNPs on PCN-224 could be clearly observed (Fig. 2B). Meanwhile, the AgNPs@PCN-224 retained a morphology similar to that of PCN-224, which proved that the introduction of AgNPs did not destroy the main framework of PCN-224. Fig. 2C presents the elemental mapping images of AgNPs@PCN-224, which show the presence of elements such as C, N, O, Zr, and Ag. Moreover, the particle-size distributions in Fig. 2D and E showed that the particle size of PCN-224 increased from 116 nm to 134 nm, with the increase in particle size indicating the successful modification of the PCN-224 by the AgNPs. Finally, according to the results of the zeta potential analysis, PCN-224 and AgNPs@PCN-224 carried positive charges of +17 and +29 mV, respectively (Fig. S2†), proving their good stability. Meanwhile, the increase in potential

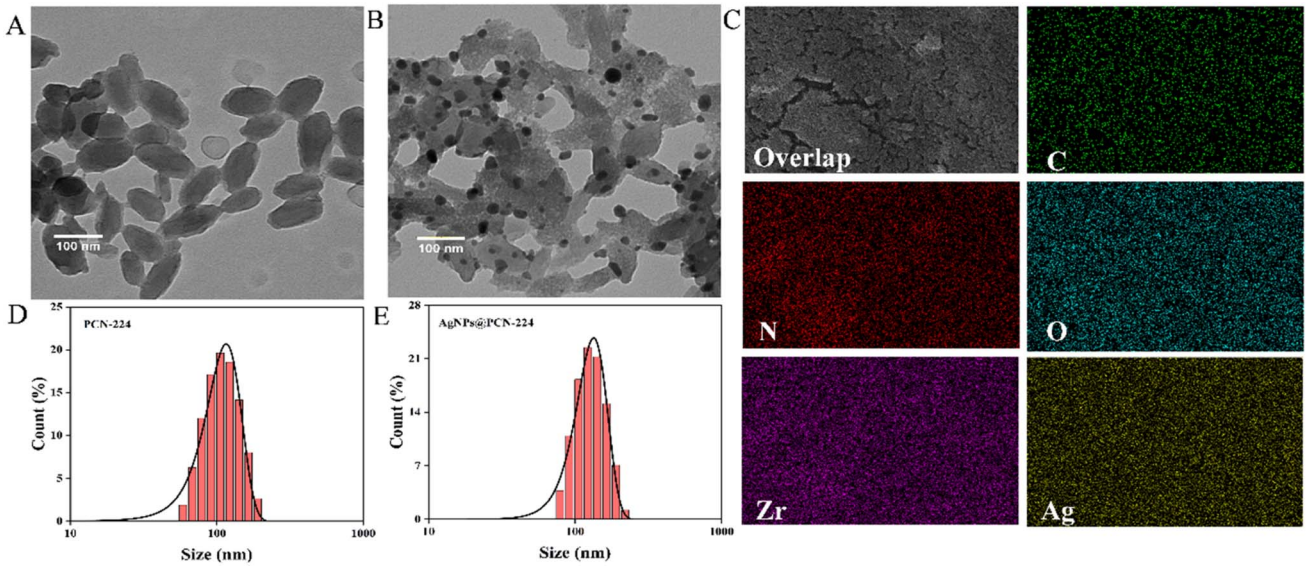

Fig. 2 TEM images of (A) PCN-224 and (B) AgNPs@PCN-224. (C) Elemental mapping images of AgNPs@PCN-224. Particle-size distributions of (D) PCN-224 and (E) AgNPs@PCN-224.

indicated that the modification by AgNPs improved the stability of the material. In summary, the successful synthesis of pure PCN-224 with good stability and its successful modification by AgNPs were confirmed.

Subsequently, a comprehensive analysis of the physical properties of the materials was conducted. As illustrated in Fig. 3A, the X-ray diffraction (XRD) pattern of the synthesized PCN-224 exhibited remarkable congruence with the standard powder diffraction card. Distinct crystalline diffraction peaks could be observed at 4.8°, 5.8°, 7.1°, 8.3° and 9.8°. These peaks were in excellent agreement with those reported in the literature, providing unequivocal evidence of the successful synthesis of pure PCN-224.[43] For AgNPs@PCN-224, the dominant characteristic peaks typical of PCN-224 were clearly discernible. Moreover, its XRD pattern bore a striking resemblance to that of PCN-224. The inset in the XRD pattern figure (Fig. 3A) revealed the emergence of two characteristic crystal planes of AgNPs in the high-angle domain at 38.1° and 46.2°. Collectively, these findings confirmed the successful synthesis of AgNPs@PCN-224. Evidently, the introduction of AgNPs did not undermine the structural integrity of PCN-224. This conclusion was in full accordance with the results obtained from the TEM analysis.

Detailed analysis of the obtained infrared (FT-IR) spectra was performed to determine the functional groups and structures of each material (Fig. 3B). First, the porphyrin ligand (TCPP) exhibited symmetric and asymmetric vibrations peaks from the C═O bond of the COO^- group at 1416 and 1603 cm^{-1}. The characteristic vibration of the Zr–OH bond of $ZrOCl_2$, which provided the metal cluster, was located at 748 cm^{-1}. In addition, the absorption peaks at 3071, 1688, 1425, 1289, 939 and 550 cm^{-1} were attributed to the benzene and pyrrole rings of benzoic acid, and included C–H bonds, C═O bonds, benzene ring backbones, C–O–C bonds, distorted peaks of pyrroles, and C–H peaks of phenyl biased bonds. A closer look at the spectrum of PCN-224 showed that the characteristic absorptions of C═O, C–N, and Zr–OH bonds appeared at 1667, 1429, and 649 cm^{-1}. Additionally, bonds belonging to the benzene ring were observed between 1400 and 1649 cm^{-1}. Meanwhile, the peak of –COOH near 949 cm^{-1} disappeared, indicating that the carboxyl group on the porphyrin ligand was fully coordinated to the metal zirconium ion. The FT-IR spectrum of the AgNPs@PCN-224 was similar to that of the pure PCN-224, whereas the –OH bonds at 3455 cm^{-1} and $-NH_2$ in the range of 600–750 cm^{-1} proved the synthesis of the AgNPs. In conclusion, the successful modification of PCN-224 by silver nanoparticles was demonstrated. The pore structure and adsorption properties of the materials were further confirmed through N_2 adsorption–desorption tests. As shown in Fig. 3C, according to the IUPAC classification, the curves for both PCN-224 and AgNPs@PCN-224 could be classified as Type I isotherms, indicating that they were mesoporous materials. However, there was a significant decrease in the BET surface area, which was attributed to the loading of AgNPs on the surface of PCN-224. The particle-size distributions in Fig. 3D showed that the average pore diameters were 2.51 and 2.68 nm, respectively, suggesting that the large-sized AgNPs only modified the surface of the material. In conclusion, these results indicated the successful synthesis of AgNPs@PCN-224. Meanwhile, the large BET surface area of 664.2 $m^2\ g^{-1}$ of PCN-224 facilitated the loading of AgNPs.

In addition, the thermal stability of PCN-224 was analyzed (Fig. S3†). The results showed that PCN-224 was stable in the range of 200 °C to 450 °C without serious mass loss, with its high thermal stability of up to 500 °C being sufficient for daily use.

Finally, the optical properties of the materials were studied. Upon observation by UV absorption spectroscopy, PCN-224 and AgNPs@PCN-224 exhibited similar spectra, indicating that the

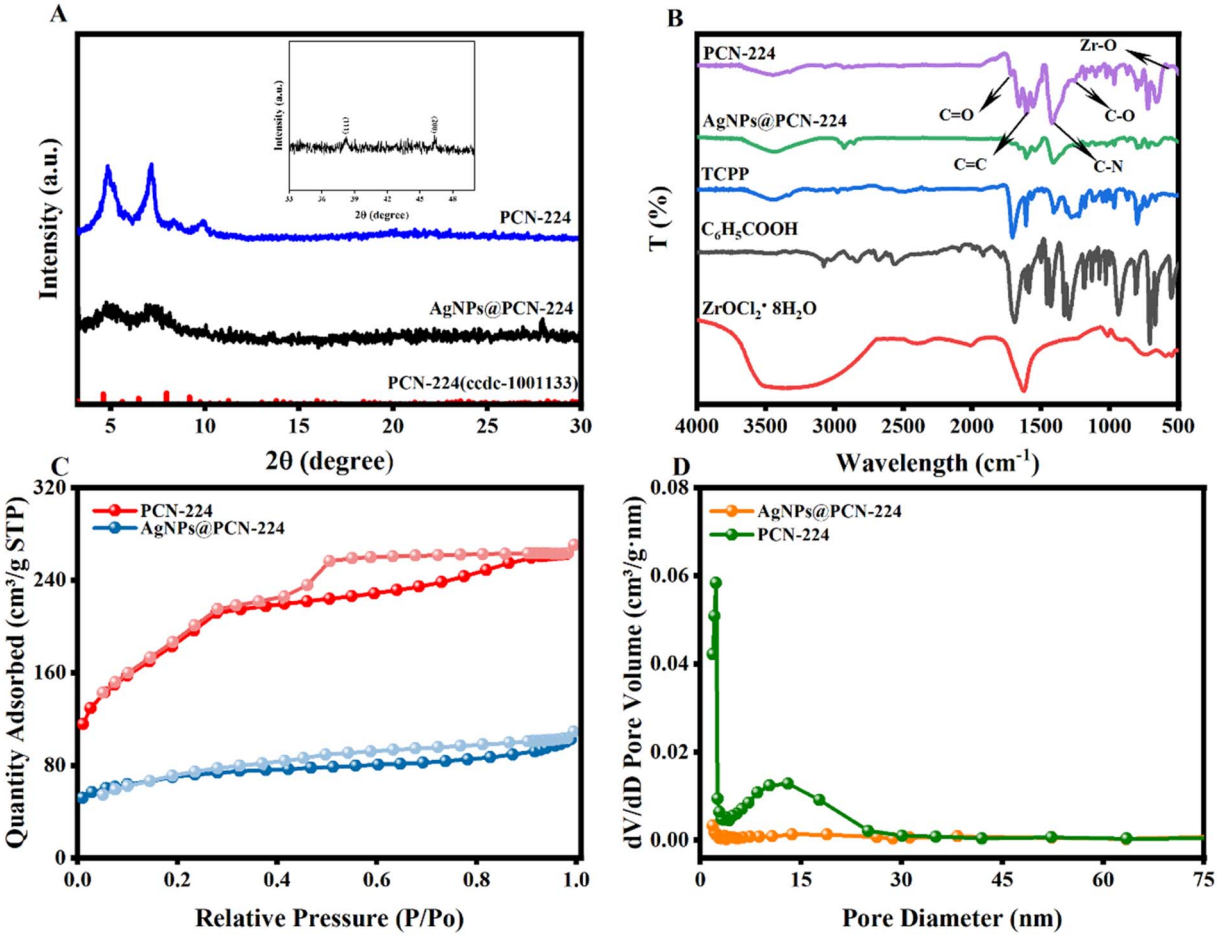

Fig. 3 (A) X-ray diffraction patterns, (B) Fourier transform infrared spectroscopy (FTIR) spectra, (C) N_2 adsorption–desorption isotherms, and (D) pore size distribution diagrams of PCN-224 and AgNPs@PCN-224.

loading of AgNPs did not alter the structure of PCN-224, while it also inherited their fluorescence properties (Fig. 4A). This was consistent with the TEM images. Additionally, typical absorption due to the conjugated structure of porphyrin molecules appeared in the range of 500–700 nm. The primary observation focused on the absorption of the Q-band, wherein weak absorptions were observed at 513, 553, 619, and 661 nm. However, it was noteworthy that AgNPs@PCN-224 showed a slight redshift and spectral broadening. This was speculated to be due to two factors: first, the noble metal nanoparticle properties of the AgNPs, which caused surface plasmon resonance; second, the high extinction coefficient of the AgNPs, which enhanced UV absorption.[44,45] Fig. 4B shows the fluorescence emission spectrum of PCN-224, where it can be observed that its maximum fluorescence emission was located at 661 nm. This was verified by three-dimensional fluorescence spectroscopy (Fig. 4C). The results confirmed that under excitation at 420 nm, the maximum fluorescence emission occurred at 661 nm, which was consistent with the aforementioned results.

Possible detection mechanism of AgNPs@PCN-224

The mechanism of fluorescence quenching was investigated. As observed from Fig. 4A, there was no change in the ultraviolet absorption spectrum before and after the addition of hydrogen peroxide. Therefore, the static quenching mechanism could be first ruled out. The fluorescence lifetimes before and after the addition of AgNPs were measured simultaneously (Fig. S4†). The results showed that the fluorescence lifetime remained basically unchanged. Therefore, it was determined that the mechanism was dynamic quenching, and it was speculated that an inner filter effect (IEF) existed. In addition, Fig. 5 shows that within the visible light range, there was a distinct overlap between the absorption curve of the AgNPs and the emission curve of PCN-224. In conclusion, it is speculated that the mechanism involved FRET and IEF.

In order to evaluate the feasibility of using AgNPs@PCN-224 for the detection of histamine, it was necessary to eliminate the influence of the substrates (DAO and histamine) on the fluorescence of PCN-224 and AgNPs@PCN-224. As shown in Fig. S5,† after the addition of DAO and histamine separately, the fluorescence intensities of PCN-224 and AgNPs@PCN-224 remained basically unchanged. This indicated that the fluorescence intensity of AgNPs@PCN-224 was solely caused by the product hydrogen peroxide (H_2O_2). At this point, the feasibility of AgNPs@PCN-224 was investigated by directly introducing H_2O_2 (Fig. 5B). It could be seen that the pure PCN-224 had

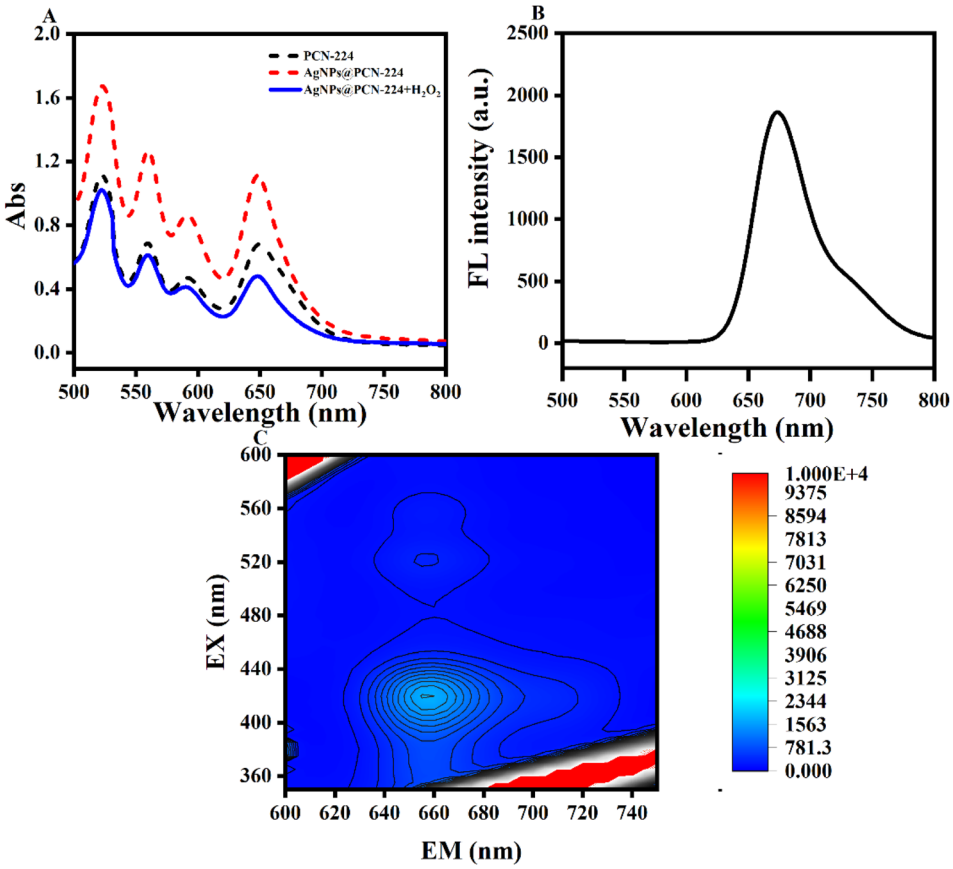

Fig. 4 (A) UV-vis spectra of PCN-224 and AgNPs@PCN-224 before and after H_2O_2 was added. (B) Fluorescence emission spectrum of PCN-224. (C) Three-dimensional fluorescence spectrum of PCN-224.

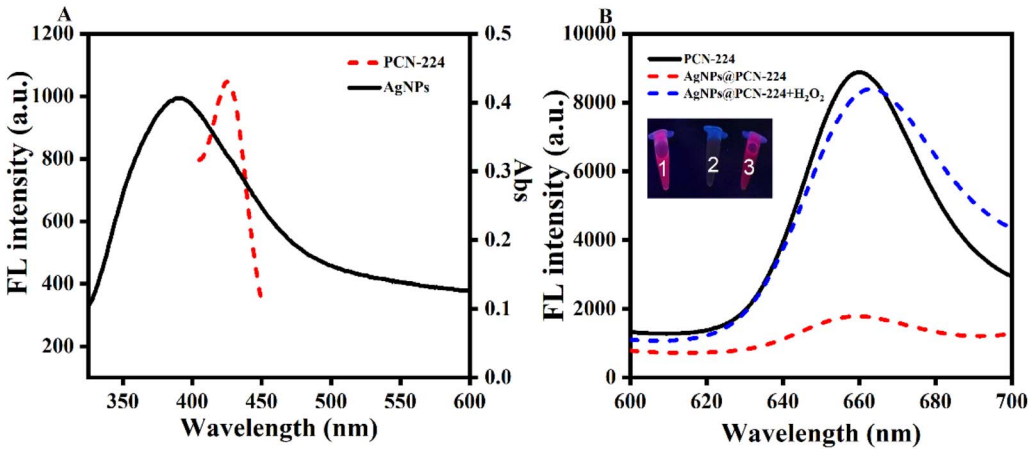

Fig. 5 (A) UV-vis spectrum of AgNPs and fluorescence emission spectrum of PCN-224. (B) Fluorescence spectra of PCN-224 and AgNPs@PCN-224 before and after H_2O_2 was added; inset shows physical drawings of the samples under UV lamp irradiation, marked as 1, 2, and 3, respectively.

a strong fluorescence emission at 661 nm and a bright red color under UV light (see the inset of Fig. 5B, tube 1). After modification with the silver nanoparticles induced the FRET and IEF processes, the fluorescence of AgNPs@PCN-224 emerged along with a slight redshift, which showed weak fluorescence at 663 nm, while no obvious fluorescence color could be seen under UV light (see the inset of Fig. 5B, tube 2). After the addition of H_2O_2, AgNPs were exfoliated from PCN-224, the FRET process was inhibited, and the fluorescence of AgNPs@PCN-224 returned to a level similar to that of PCN-224, with a brighter red fluorescence color observed under UV light (see the inset of Fig. 5B, tube 3). Additionally, the consistency between the color changes and the fluorescence intensity changes in the illustrations further proved that this probe was

suitable for the fluorescent detection and visual recognition of H_2O_2 and histamine.

To exclude the influence of H_2O_2 on the fluorescence, we investigated the variation in fluorescence intensity at different concentrations of H_2O_2 (Fig. S6†). It was found that there was no change in fluorescence intensity as the H_2O_2 concentration increased from 0 to 20 mM, with the curves nearly overlapping. The above finding indicated that H_2O_2 had no direct impact on the fluorescence of PCN-224. The fluorescence change was based on the reducing effect of H_2O_2 on the AgNPs, which in turn affected the quenching effect of the AgNPs on PCN-224.

Detection of H_2O_2

H_2O_2 is easily decomposed, and both the pH and temperature affect its stability and effectiveness, and thereby can reduce the sensitivity of the probe, thus requiring optimization of the detection conditions. Fig. S7a† shows the fluorescence response was affected under both neutral and alkaline conditions, which was due to the partial decomposition of H_2O_2 under alkaline conditions, resulting in the inhibition of reduction. Therefore, pH 6.5 was chosen as the reaction environment for H_2O_2. Next, temperature optimization was carried out in the range of 15–55 °C, and it could be seen the fluorescence response reached its maximum value at 35 °C (Fig. S7b†). Because the increase in temperature accelerated the decomposition of H_2O_2, 35 °C was used as the temperature for the subsequent experiments. Fig. S7c† shows that AgNPs@PCN-224 had a fast and good fluorescence response to H_2O_2, whereby the fluorescence increased rapidly within 5 min and then stabilized at 15 min. In summary, the optimum pH, time and temperature for the detection of H_2O_2 by the AgNPs@PCN-224 probe were 6.5, 5 min and 35 °C, respectively.

Next, the detection performance for H_2O_2 was determined by measuring the change in fluorescence intensity within a specific concentration range (0–100 nM) (Fig. S8†). It was clear that an increase in H_2O_2 concentration led to a significant enhancement in fluorescence (Fig. S8a†). Between 10 and 100 nM, there was a clear linear relationship between the fluorescence response ($F - F_0$) and the concentration, which could be expressed as $F - F_0 = 10.657x - 92.708$ ($R^2 = 0.954$), where F and F_0 represent the initial and final fluorescence intensities before and after the addition of H_2O_2 at 661 nm, respectively. Finally, the LOD was calculated to be 3.3 nM (S/N = 3), indicating that this probe possessed sufficient sensitivity for detecting H_2O_2.

In addition, its stability and selectivity were investigated (Fig. S9†). The specificity of the probe was then evaluated with three organic reagents (ethylene glycol, methanol and ethanol). Fig. S9a† shows that only H_2O_2 could significantly enhance the fluorescence, while the other substances caused negligible changes. Furthermore, the fluorescence intensity was continuously measured over a period of 20 days, and the results

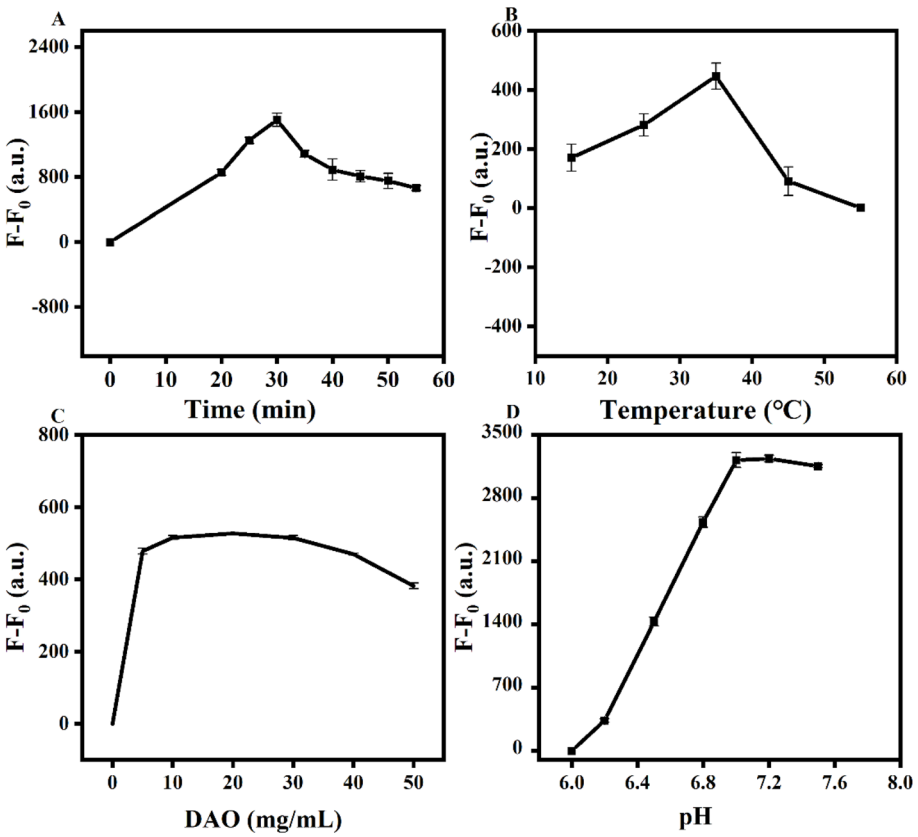

Fig. 6 (A) Effect of time, (B) temperature, (C) concentration of DAO and (D) pH on the fluorescence response. All the experiments were performed in triplicate.

remained largely unchanged (Fig. S9b†). In conclusion, this developed probe has good stability and selectivity.

Optimization of the detection conditions

As previously demonstrated, the detection principle involved utilizing the oxidizing action of H_2O_2 to reduce AgNPs to Ag^+, resulting in a change in fluorescence. The source of H_2O_2 can be the catalytic action of diamine oxidase on diamines, with histamine being the focus of this study. The key to the enzymatic reaction was a stable enzymatic activity, so in this study, the DAO activity was related to the sensitivity of the probe, and its activity mainly depended on the reaction time, pH, temperature and DAO concentration. Therefore, to optimize the above influencing factors, histamine was dissolved in PBS and used as the reaction solution.

The optimum time for the incubation of histamine with DAO was first determined and the results are shown in Fig. 6A. The fluorescence response increased rapidly at the beginning of the incubation, reaching a maximum at 30 min, but then leveled off as the catalytic reaction neared completion. Therefore, the incubation time selected for the subsequent detection was 30 min. As can be seen from Fig. 6B, DAO had an optimum temperature, and the catalytic activity reached its maximum at 35 °C, which corresponded to the maximum fluorescence response. Both low and high temperatures affected its catalytic efficiency, so 35 °C was selected as the optimum incubation temperature. Meanwhile, the system pH also had a large effect on DAO activity, with Fig. 6C clearly showing that the DAO activity was the highest under neutral conditions, so pH 7 was determined to be the optimal pH value. In addition, the DAO concentration was also a key factor affecting the enzymatic reaction. Fig. 6D shows that the fluorescence response peaked at 20 mg mL^{-1}, while further increasing the concentration led to a decrease in fluorescence and even saturation. Therefore, 20 mg mL^{-1} was used as the optimal concentration of DAO for the catalytic reaction of histamine in the further experiments.

Detection of histamine

As mentioned above, the fluorescence of PCN-224 was unaffected by H_2O_2, thus the fluorescence change could only be attributed to the reduction of AgNPs@PCN-224 by H_2O_2. Which was beneficial for ensuring the accuracy of the subsequent experiments.

Under optimized conditions, the detection performance of the constructed probes was examined. As shown in the fluorescence spectrum of Fig. 7A, the fluorescence intensity gradually enhanced with the increase in histamine concentration in the range of 0 nM to 1 mM. Accordingly, the linear relationship between the fluorescence response ($\Delta F = F - F_0$) and histamine concentration was derived as $Y = 43.25 \log C + 281.4$, with a correlation coefficient R^2 of 0.9527, where F_0 and F correspond to the initial and final fluorescence intensities before and after histamine addition. The limit of detection (LOD) was calculated as 0.033 nM according to the formula LOD $= 3\sigma/K$, where σ is the standard deviation, and K is the slope of the calibration curve. This LOD is much lower than the value reported in some other recently published methods (see Table S1†). In addition, since cadaverine, putrescine and histamine in aquatic products are all diamines, and the reaction of equal amounts of diamines with diamine oxidase can produce equal amounts of H_2O_2, it was further hypothesized that the probe would be suitable for other diamines, such as cadaverine and putrescine.

Selectivity and stability of AgNPs@PCN-224

Selectivity and stability are key parameters for assessing the performance of analytical methods in practical applications. To ensure the specificity of the assay, it was necessary to confirm that other chemicals with similar structures or those possibly co-existing in a fish sample would not cause a response by the probe. Therefore, some structural analogs (cysteine (Cys), phenylalanine (Phe), glycine (Gly), *n*-hexane), inorganic anions (SO_4^{2-}, CO_3^{2-}) and metal cations (Ca^{2+} and Fe^{3+}) and other potential interfering substances were selected for determination under the same operating procedures. Fig. 8A shows that the addition of BAs (His, Cad, Put) resulted in a significant fluorescence response, which was much larger than that of the other interfering groups. Additionally, there was no difference among the BAs. The stability was tested by storage at 4 °C for 20 days. Fig. 8B shows that the fluorescence intensity remained basically unchanged throughout the 20 days, indicating that the probe had good stability for at least 20 days. The above results indicated that the selectivity and stability of AgNPs@PCN-224 probe could meet the requirements for histamine detection.

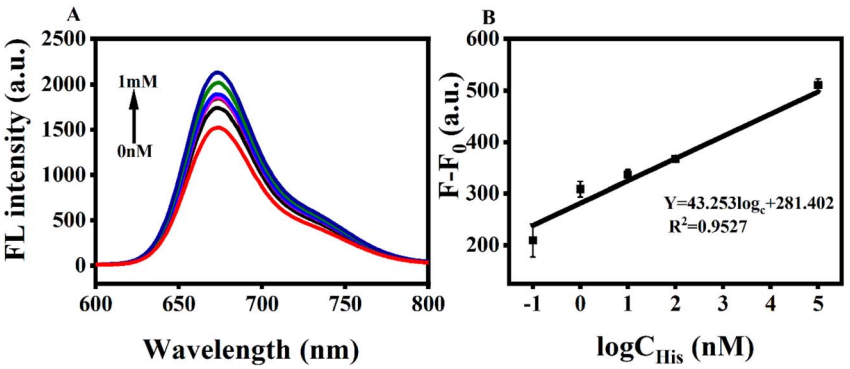

Fig. 7 (A) Fluorescence determination of histamine (0 nM to 1 mM) and (B) corresponding calibration curve.

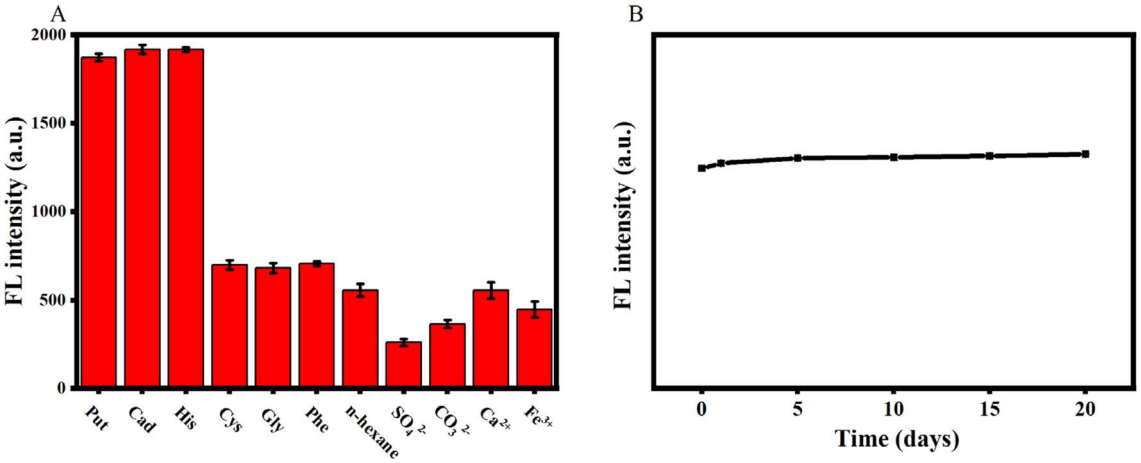

Fig. 8 (A) Specificity and (B) stability of AgNPs@PCN-224.

Table 1 Bioamine-labelled recovery experiment

Sample no.	Added (ng mL^{-1})	Found (ng mL^{-1}) ($x \pm s$, $n = 3$)	RSD (%)	Recovery (%)
1	10	11 ± 0.4	7.3	110
2	100	103 ± 2	2.4	103
3	1000	983.28 ± 28	2.9	98

Real sample detection

To evaluate the applicability and reliability of the established AgNPs@PCN-224 fluorescence probe for detecting histamine in practical applications, it was applied to detect histamine in grass carp samples. Here, a certain concentration of histamine standard solution was added to the samples, and the assay was performed according to the optimal conditions and the methods described above. As shown in Table 1, the recoveries of biogenic amines ($n = 3$) were as high as 98–110%, with relative standard deviations (RSD) of 2.4–7.3%. The results indicated that the AgNPs@PCN-224 fluorescent probe designed in this study was suitable for the detection of histamine in real food samples.

Conclusions

To sum up, in this study, a novel fluorescence probe (AgNPs@PCN-224) was designed and optimized, which involved a fluorescence response mode based on the enzyme-mediated turn-on of a luminescent metal–organic framework modified with silver nanoparticles. On the one hand, the fluorescence signal originated from the material itself simplified the design route of the probe and gave it a high stability and a high quantum yield. On the other hand, the selectivity and sensitivity for histamine and hydrogen peroxide detection were enhanced by introducing a cascade reaction between the amine and enzyme. It is also worth noting the future potential of luminescent metal–organic frameworks (LMOFs). As the ideal sensing platform, they have gradually become the preferred choice in the field of optical sensing, and their application areas are expanding. Researchers need to seize the opportunity to further explore and develop luminescent metal–organic frameworks.

Data availability

Data will be made available on request.

Author contributions

Mei Zhou: methodology, software, data curation, investigation, formal analysis, writing – original draft, preparation. Simiao Zhang: software, data curation. Shishuang Wang: investigation, supervision. Yutong Huang: software, data curation. Xiaokang Xu: software, data curation. Weiqing Sun: investigation, supervision. Qiaozhen Liu: software, data curation. Jing Ma: writing – review & editing, supervision, project administration, funding acquisition.

Conflicts of interest

There are no conflicts to declare.

Acknowledgements

Mei Zhou gratefully acknowledges financial support from the Natural Science Foundation of Hubei Province (2024AFB981) and the National Natural Science Foundation of China (32360622).

References

1 I. Obara, V. Telezhkin, I. Alrashdi and P. L. Chazot, *Br. J. Pharmacol.*, 2020, **177**, 580–599.
2 K. B. Biji, C. N. Ravishankar, R. Venkateswarlu, C. O. Mohan and T. S. Gopal, *J. Food Sci. Technol.*, 2016, **53**, 2210–2218.

3 R. Shi, S. Feng, C. Y. Park, K. Y. Park, J. Song, J. P. Park and T. J. Park, *Biosens. Bioelectron.*, 2020, **167**, 12519.
4 Y. Huang, S. Zhang, M. Zhou, X. Xu, W. Sun, J. Ma and L. Wu, *Int. J. Mol. Sci.*, 2024, **26**(1), 139.
5 Y. Qin, P. Huang and F. Y. Wu, *Sens. Actuators, B*, 2022, **365**, 131911.
6 B. Zhang, J. Zhang, Y. Lang, Z. Wang, D. Cai, X. Yu and X. Lin, *Food Chem.*, 2024, **433**, 137281.
7 G. Wu, X. Dou, D. Li, S. Xu, J. Zhang, Z. Ding and J. Xie, *Biosensors*, 2022, **12**(3), 161.
8 C. Ruiz-Capillas and A. M. Herrero, *Foods*, 2019, **8**(2), 62.
9 S. Swathy, G. S. Pallam and K. G. Kumar, *Talanta*, 2023, **256**, 124321.
10 Z. Wu, E. Xu, A. Jiao, Z. Jin and J. Irudayaraj, *RSC Adv.*, 2017, **7**, 44933–44944.
11 X. Miao, C. Wu, F. Li and M. Zhang, *Adv. Funct. Mater.*, 2023, **33**, 2212980.
12 J. Xin, X. Wang, N. Li, L. Liu, Y. Lian, M. Wang and R. S. Zhao, *Food Chem.*, 2020, **330**, 127255.
13 D. Lancet and I. Pecht, *Biochemistry*, 1977, **16**(23), 5150–5157.
14 A. Romano, H. Klebanowski, S. La Guerche, L. Beneduce, G. Spano, M. L. Murat and P. Lucas, *Food Chem.*, 2012, **135**, 1392–1396.
15 Y. J. Zhang, Y. Zhang, Y. Zhou, G. H. Li, W. Z. Yang and X. S. Feng, *J. Chromatogr. A*, 2019, **1605**, 360361.
16 A. Önal, *Food Chem.*, 2007, **103**(4), 1475–1486.
17 H. Vasconcelos, J. M. de Almeida, A. Matias, C. Saraiva, P. A. Jorge and L. C. Coelho, *Trends Food Sci. Technol.*, 2021, **113**, 86–96.
18 V. R. Heerthana and R. Preetha, *Rev. Fish. Sci.*, 2019, **11**, 220–233.
19 M. A. Alonso-Lomillo, O. Domínguez-Renedo, P. Matos and M. J. Arcos-Martínez, *Anal. Chim. Acta*, 2010, **665**, 26–31.
20 V. Kumar and K. H. Kim, *Environ. Pollut.*, 2022, **99**, 118824.
21 J. Ma, L. Wu, Z. Li, Z. Lu, W. Yin, A. Nie, H. Han, *et al.*, *Anal. Chem.*, 2018, **90**(12), 7415–7421.
22 D. Yao, Y. Wang and H. Li, *Sens. Actuators, B*, 2020, **305**, 127451.
23 Y. Chen, X. Yang, C. Lu, Z. Yang, W. Wu and X. Wang, *Chin. Chem. Lett.*, 2023, **34**, 108099.
24 F. Y. Yi, D. Chen, M. K. Wu, L. Han and H. L. Jiang, *ChemPlusChem*, 2016, **81**, 675–690.
25 Y. Feng, Y. Wang and Y. Ying, *Coord. Chem. Rev.*, 2021, **446**, 214102.
26 H. Zhang, P. Xiong, G. Li, C. Liao and G. Jiang, *TrAC, Trends Anal. Chem.*, 2020, **131**, 116015.
27 F. Z. Chen, Y. J. Li, M. Zhou, X. X. Gong, Y. Gao, G. Cheng, D. M. Han, *et al.*, *Appl. Catal., B*, 2023, **328**, 122517.
28 E. Kouti, A. Tsiasioti, C. K. Zacharis and P. D. Tzanavaras, *Microchem. J.*, 2021, **168**, 106513.
29 W. Cheng, X. Tang, Y. Zhang, D. Wu and W. Yang, *Microchem. J.*, 2021, **12**, 268–282.
30 H. C. Gulbalkan, Z. P. Haslak, C. Altintas, A. Uzun and S. Keskin, *Chem. Eng. J.*, 2022, **428**, 131239.
31 C. Pettinari, R. Pettinari, C. Di Nicola, A. Tombesi, S. Scuri and F. Marchetti, *Coord. Chem. Rev.*, 2021, **446**, 214121.
32 M. Miao, L. Mu, S. Cao, Y. Yang and X. Feng, *Carbohydr. Polym.*, 2022, **291**, 119587.
33 H. S. Wang, *Coord. Chem. Rev.*, 2017, **349**, 139–155.
34 A. Loiseau, V. Asila, G. Boitel-Aullen, M. Lam, M. Salmain and S. Boujday, *Biosensors*, 2019, **9**(2), 78.
35 H. D. Beyene, A. A. Werkneh, H. K. Bezabh and T. G. Ambaye, *Sustainable Mater. Technol.*, 2017, **13**, 18–23.
36 S. Zhang, N. Zhang, S. Wang, Z. Li, W. Sun, M. Zhou, J. Ma, *et al.*, *Microchem. J.*, 2023, **190**, 108664.
37 J. Ma, W. Wang, Y. Li, Z. Lu, X. Tan and H. Han, *Anal. Chem.*, 2021, **93**, 2090–2096.
38 H. J. Cho, E. Kang, S. Kim, D. C. Yang, J. Nam, E. Jin and W. Choe, *Inorg. Chem.*, 2021, **60**, 16966–16976.
39 W. Zhou, Z. Hu, J. Wei, H. Lu, H. Dai, J. Zhao, R. Guo, *et al.*, *Compos. Commun.*, 2022, **33**, 101221.
40 L. Wang, Y. Pan, Z. Wang, Y. Wang and X. Wei, *ACS Appl. Mater. Interfaces*, 2023, **15**, 44109–44118.
41 Y. W. Zhang, W. S. Liu, J. S. Chen, H. L. Niu, C. J. Mao and B. K. Jin, *Sens. Actuators, B*, 2020, **321**, 128456.
42 Z. Zhang, K. Pei, Z. Yan and J. Chen, *Luminescence*, 2021, **36**(1), 215–221.
43 R. Shi, D. Lv, Y. Chen, H. Wu, B. Liu, Q. Xia and Z. Li, *Sep. Purif. Technol.*, 2018, **207**, 262–268.
44 L. Mattsson, J. Xu, C. Preininger, B. T. S. Bui and K. Haupt, *Talanta*, 2018, **181**, 190–196.
45 Z. Xu, Q. Li, Y. Wang, S. Yu, Y. Jiao, L. Wen and Y. Cheng, *Sens. Actuators, B*, 2023, **377**, 133037.